A combined friction energy and tribo-oxidation formulation to describe the high temperature fretting wear response of a cobalt based alloy

Alixe Dreano, Siegfried Fouvry, Gaylord Guillonneau

A combined friction energy and tribo-oxidation formulation to describe the high temperature fretting wear response of a cobalt-based alloy

Alixe Dreano*, Siegfried Fouvry, Gaylord Guillonneau

University of Lyon, Ecole Centrale de Lyon, LTDS UMR 5513 CNRS, Ecully, France

* alixe.dreano@ec-lyon.fr

Abstract

A cobalt-based superalloy (HS25) versus alumina contact was subjected to gross slip fretting using a cross-cylinders configuration and various tribological conditions. The present study focuses on the modelling of different wear mechanisms which mainly depend on the operating temperature.

Wear below a threshold temperature (150°C) is severe whereas a protective oxide layer is formed above the temperature transition. At low temperature, the wear process was found to be controlled by a continuous action of the oxidation of the surface and the abrasion of the latter. Wear mechanism was also showed to be strongly dependent on temperature, sliding amplitude and frequency [1]. An energetic wear law was developed to formalize the oxidative-abrasive wear mechanism displaying a good correlation with experiments.

Above the threshold temperature, the oxidative-abrasive phenomenon is not operating anymore and a protective glaze layer is formed at the interface. A tribo-sintering approach is proposed to predict the glaze layer formation for various tribological parameters. Moreover, the glaze layer protective effect was taken into consideration in the wear formulation by considering that only the friction energy dissipated before the glaze layer creation needs to be integrated. The proposed formulation showed a very good prediction of wear volumes from ambient to high temperature (600°C).

Keywords

Fretting ; friction energy formulation; abrasive wear ; glaze layer ; high temperature ; third body

Nomenclature

Material	
HS25	Haynes 25, cobalt-based alloy
Loading conditions	
P	Normal Force (N)
T	Temperature (°C)
Q	Tangential Force (N)
Q^*	Maximum tangential force (N)
N	Number of fretting cycles
N_{crit}	Critical number of cycle after which there is no more wear
N_{GL}	Number of cycle needed for the glaze layer creation
N_{eff}	Effective number of cycle
δ	Fretting displacement (µm)
δ^*	Displacement amplitude (µm)
δ_0	Sliding amplitude (µm)
$\delta_{0,crit}$	Critical sliding amplitude after which wear increases (µm)
f	Frequency (Hz)
μ	Conventional friction coefficient
μ_e	Energetic friction coefficient
$\overline{\mu_e}$	Mean energetic friction coefficient
Wear volume	
$\overline{V_{HS25}}$	HS25 missing volume (mm^3)
V	Total wear volume (mm^3)
V_ϕ, $V_\phi(T)$	Offset of wear (mm^3)
Wear modelling	
E_d	Dissipated energy or friction energy (J)
ΣE_d	Cumulated dissipated energy (J)
$\Sigma E_{d,eff}$	Effective cumulated dissipated energy (J)
α	Conventional energetic wear coefficient (mm^3/J)
α_{ox}, $\alpha_{ox}(T)$	Oxidational energetic wear coefficient ($mm^2/s^{0.5}/J$)
α^*	Apparent energetic wear coefficient (mm^3/J)
Ψ	Tribo-oxidation parameter ($mm/s^{0.5}$)
E_a	Activation energy of the oxidation process (J/mol)
K_{ox}	Oxidational wear coefficient ($mm^2.s^{0.5}/J$)
k_p, k_{p0}	Oxidation rate and pre-exponential constant (mm^2/s)
S, S_{GL}	Sintering parameter and threshold value (mm^2/s)
$t_{holding}$	Process time for sintering (s)
Subscripts	
ref	Corresponds to the reference conditions
I,II,III	Referred to domains I, II and III
1,2	Referred to the transition temperature
Others	
R	Universal constant (J/K/mol)
R^2	Coefficient of determination

1. Introduction

Fretting is usually defined as a small reciprocating displacement which can be found in many industrial systems, such as in plane turboengine. The blades/disk contact of the turbines undergoes micro-displacements at various temperatures during aircraft flight [2–5]. Cobalt-based alloys are used for their good mechanical properties and corrosion resistance [3,4]. It is therefore important to have a good understanding of wear mechanisms of cobalt superalloys and their relationship with the temperature fluctuations during fretting loads.

High temperature wear mechanisms of cobalt-based alloys have been intensively investigated over the past decades. It was shown that above a critical temperature the surface damage is changing from severe to mild wear when a compliant oxide layer acting as a solid lubricant is formed [1,4–7]. This layer is usually called “glaze layer” and drastically decreases the wear damage of the bulk surface as well as the friction coefficient [8,9]. Many authors have shown that the glaze layer is formed from the oxide debris generated at the very beginning of the test [7,10]. The glaze layer formation is promoted by the diffusive properties of oxides [6,11] during a tribosintering process [12]. The literature also shows that the glaze layer is mainly nanocristalline [13,14] but some authors have emphasized the presence of some amorphous zones [15,16] which could be the major plasticity activator of the glaze layer behavior [17]. Indeed, Viat et al. [17] showed that the very good tribological properties of the glaze layer is mainly due to its ductility at high temperature which is able to accommodate the stress induced by fretting. Jiang [7] developed a wear law considering that the wear process depends on the capacity of debris to be retained, committed, agglomerated and finally sintered together. This law showed a good prediction of mild-wear but was not able to predict the transition from severe to mild.

Until recently, there was a lack of investigations in the low-to-medium temperature domain, when the temperature is not high enough to agglomerate the oxide wear debris and thus form a protective layer. In a previous research [1], it was shown that, in the low temperature domain, severe wear process is controlled by a synergetic action of abrasion and oxidation of the surface. The wear evolution versus temperature, sliding amplitude and frequency appeared to be driven by the kinetics of contact oxidation, whereas the normal force and the total sliding distance monitored the abrasive part of the wear process. A wear law was proposed displaying a good correlation with experiments for low temperature condition (severe wear) [1].

In this work, the former oxidative-abrasive formulation [1] is derived into a friction energy wear formalism since the friction energy approach is widely considered in the literature [5,18,19]. This research, based on abrasive and oxidative considerations, provides a more physical description of the surface damage and its relation to temperature. A modified energetic wear law is proposed in order to capture the change of wear mechanism (from severe to mild wear) as a function of various tribological parameters. Above a threshold temperature, the formation of a glaze layer reducing drastically the wear process is taken into account by considering an effective dissipated friction energy. The third body protective effect is then introduced in the global formulation and results showed a very good correlation for describing the formation of such glaze layer which depends on temperature, frequency or sliding amplitude.

2. Experiments

2.1. Materials and fretting tests

The cobalt-based alloy Haynes 25 was tested against alumina in a cross-cylinders configuration, presented on Fig. 1 a), where P is the applied normal load and δ the imposed displacement. Alumina was chosen for its chemical inertness and its capacity to resist fretting wear as shown in a previous study [1]. The as-received Haynes 25 rods was heat-treated at 1185°C during 30 minutes and water quenched inducing a mean grain size of 66 µm [20]. An additional machining and grinding step was performed to obtain a radius of 4 mm with a roughness Ra equal to 0.45 µm. It induced on the HS25 surface a hard-workened layer as presented in Fig. 1 b) with a hardness 1.8 times higher than that of the bulk (nano-indentation tests not presented here). The chemical compositions and mechanical properties of the bulk materials are listed in Table 1.

Table 1: Chemical composition and mechanical properties of the studied materials

	HS25 (bulk material)	Alumina
Composition (w. %)	50.88 % Co, 20.28 % Cr, 10.16 % Ni, 14.89 % W, 2.18 % Fe, 1.39 % Mn	43.5 % O, 56.5 %0 Al
Modulus of elasticity (GPa)	225 (20°C), 181 (600°C)	310
Yield strength (MPa)	475 (25°C), 330 (540°C)	1800 (resistance to compression at 20°C)
Hardness (Hv)	251 (20°C), 171 (425°C)	1800

Fretting tests were performed on a high temperature fretting test bench presented in [1]. The Haynes 25 cylinder was fixed on a sample holder and a displacement δ with a frequency f was imposed on the alumina sample during N cycles. The sliding amplitude δ_0 is defined as the residual displacement measured when the tangential force Q is equal to 0, as presented in Fig. 1 c). When Q = 0, both samples and test apparatus tangential accommodation are reduced: hence, δ_0 well approximates the effective sliding displacement operating in the interface. In the present investigation, a constant sliding amplitude δ_0 was imposed during the tests by continuously adjusting the displacement amplitude δ^* so that δ_0 remains constant.

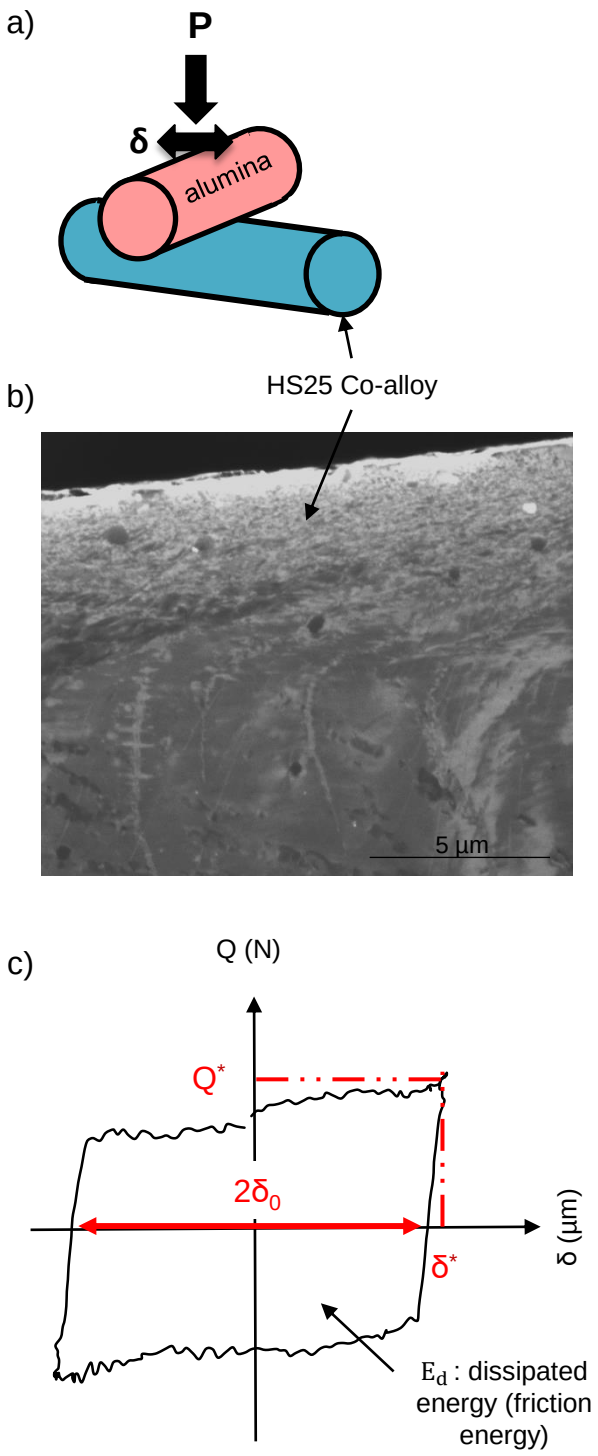

Fig. 1: (a) Cross-cylinders contact configuration, (b) SEM cross-sectional observation of the HS25 microstructure before the fretting tests and (c) fretting cycle plotted from experimental data

2.2. Loading conditions

To quantify the wear response of the studied contact, a cross-experimental strategy was adopted, centered on a reference point: P_{ref} = 50 N; f_{ref} = 50 Hz; $\delta_{0,\,ref}$ = ± 20 µm; N_{ref} = 200 000. When no specification is given, the parameters are set to their reference. Fig. 2 shows the experimental procedure where the sliding amplitude varies from ± 10 µm to ± 140 µm, the normal force between

30 and 130 N and the frequency between 5 and 80 Hz. In addition, fretting tests were carried out from 5000 to 300000 cycles for the reference test.

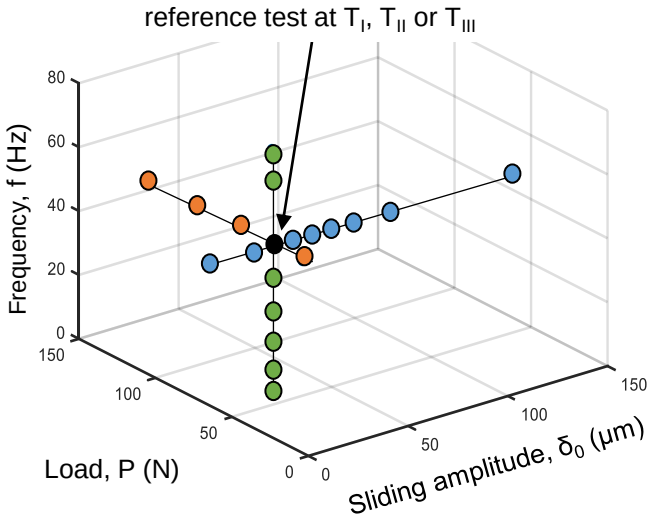

Fig.2: Cross-experimental strategy

Wear tests were also performed in a controlled temperature environment where temperature at the interface was maintained between 25 and 600°C. The cross-experimental strategy was carried out for three reference temperatures: T_I = 100°C for the low temperature domain, T_{II} = 230°C for the medium temperature domain and T_{III} = 575°C for the high temperature domain. Some tests were duplicated and the error bars are standard deviations. Some bars are not seen in the graphs due to the very low error (especially at high temperature).

2.3. Friction and wear measurements

In this study, the energetic friction coefficient over a fretting cycle was used and defined according to Eq. 1:

$$\mu_e = \frac{Ed}{4P\delta_0} \quad (1)$$

The energetic friction coefficient is better to estimate friction operating during fretting cycle than the conventional one (µ = Q/P) which tends to overestimate friction due to plowing [5].

The dissipated energy E_d was calculated through the fretting cycle (Fig. 1 b)) and expressed as the total area of the fretting loop. For further calculations, the cumulated friction energy over one fretting test will be approximated by Eq. 2, assuming constant sliding condition (P and δ_0 are constant during the tests).

$$\sum E_d = \sum_{i=1}^{N} E_{d,i} = 4P\overline{\mu_e}\delta_0 N \quad (2)$$

Where $\overline{\mu_e}$ is the mean energetic friction coefficient. After tests, the samples were cleaned in an ultrasonic bath with ethanol and optically observed. 3D surface profiles were also performed on both HS25 and alumina (Veeco optical profilometry). After a numerical subtraction of the cylindrical shape of the samples (Fig. 3), the fretting scars of HS25 (Fig. 3 a)) and alumina (Fig. 3 b)) were analyzed. As

previously shown [1], the alumina rods do not present missing wear volumes but only a very thin transferred layer of HS25 (see Fig. 3 b) and [1]). The total wear volume was defined as the total missing wear volume which is then equal to the missing wear volume of the HS25 sample (Fig. 3 a)).

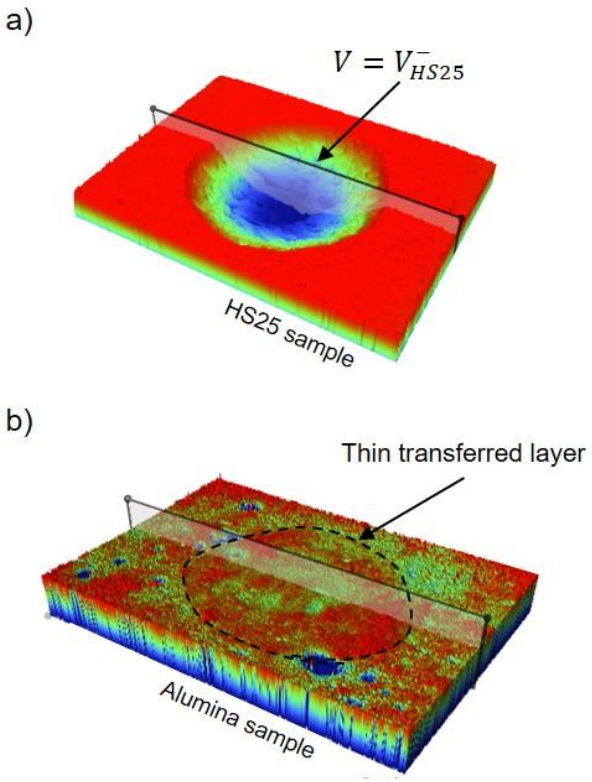

Fig.3: 3D surface profiles of the wear tracks on (a) HS25 and (b) alumina after numerical subtraction of the cylindrical shape

2.4. Wear tracks characterization

Cross-sections of the wear scars were prepared by cutting, mounting, grinding and polishing. Surface and cross-section observations were performed with a FEG SEM (Tescan) equipped with an EDX detector (Oxford Instruments) for elemental chemical analyses. Accelerating voltage is equal to 20 kV for EDX quantifications and 5 kV for morphological observations. Metallic oxide characterizations were performed with a micro-Raman vibrational spectroscopy (Horiba) at the 785 nm incident radiation wavelengths.

3. Tribological results

3.1. Temperature-dependent wear mechanisms

Fig. 4 a) shows the evolution of the friction coefficient with fretting cycles for the three reference temperatures: 100°C, 230°C and 575°C.

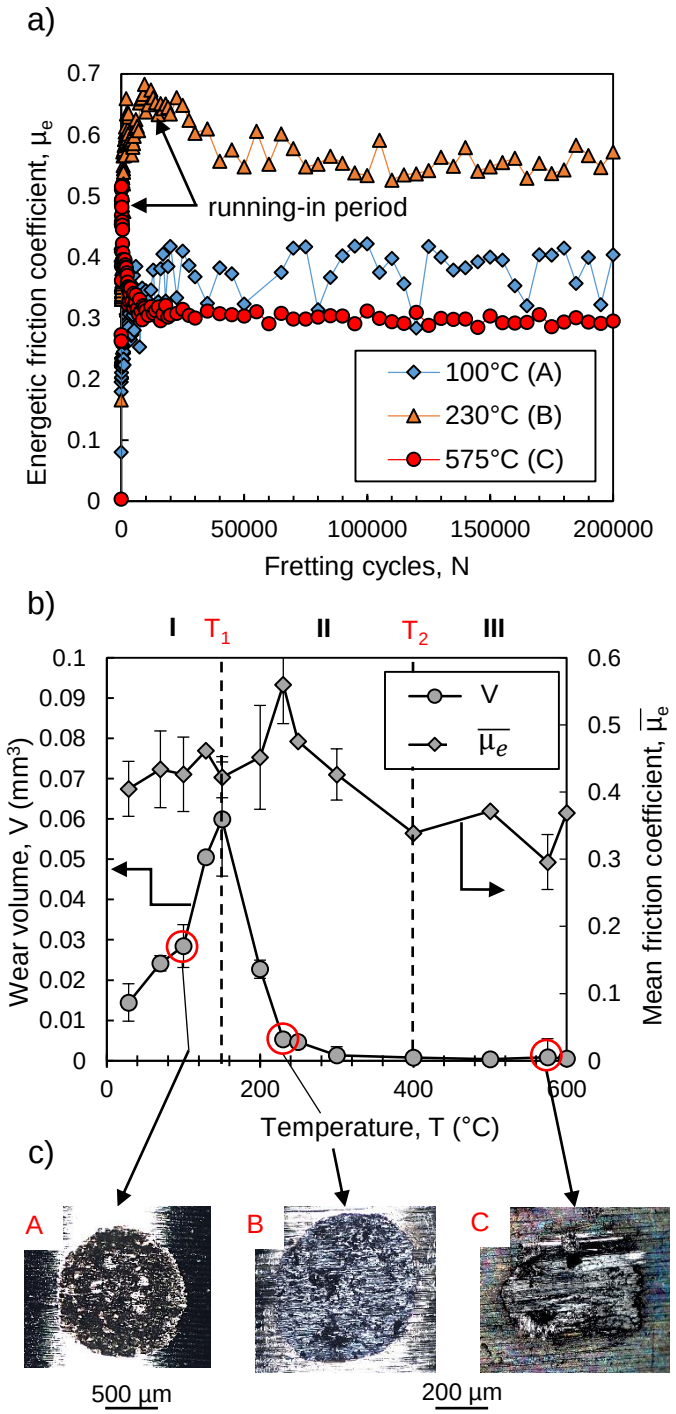

Fig. 4: (a) Evolution of the energetic friction coefficient with fretting cycles for the three reference temperatures: 100°C, 230°C and 575°C, (b) effect of temperature on the wear volume and the mean friction coefficient and (c) associated wear tracks

At 100°C, the friction coefficient evolution is unstable and oscillates a lot during the test. At 230°C and 575°C, the evolution is more stable with fretting cycles and present an increasing friction coefficient during the running-in period which may be related to the enhanced adhesion of the surfaces due to temperature. Fig. 4 b) displays the total wear volume and the mean energetic friction coefficient with temperature. As previously observed [1,5], the wear volume curve displays three domains. In domain I, wear increases with temperature up to a transition temperature T_1 equal to

150°C. In this domain, the friction coefficient does not seem to show a particular trend. The optical image associated with domain I in Fig. 4 c) shows the presence of abrasive grooves inside the wear track. Above the T_1 temperature, the wear track is brighter and smaller than in domain I and wear falls down as well as the friction coefficient. It is interesting to notice that the decrease in friction coefficient takes place for temperatures higher than 230°C which is eighty Celsius degrees higher than the temperature at which the wear volume decreases (150°C). This phenomenon was not observed previously and will be discussed later. Above 400°C, in domain III, wear is very low and the friction coefficient is stable around 0.35. The associated wear track is bright, smooth and smaller than in domain II.

To sum up, Fig. 4 shows that the wear volume, the friction coefficient and the morphological aspect of the wear tracks are very sensitive to the temperature. The T_1 transition temperature shows radical change in the wear mechanism involved in the HS25/alumina interface. It was shown that wear in domain I is driven by a synergetic interaction of abrasion and oxidation of the fretted interface [1]. Transition T_2 is well defined by the stabilization of the friction coefficient and the wear volume, reaching a very low value. This is due to the formation of a protective and lubricant layer at the interface as classically observed for metallic alloys [15,17]. Finally, domain II is a transition domain between the oxidative-abrasive process and the glaze layer protection.

3.2. Parametric study of wear

Fig. 5 shows the wear volume evolution with various tribological parameters: a) fretting cycle, b) frequency, c) normal force and d) sliding amplitude. The effect of these parameters are tested for the three reference temperatures.

In Fig. 5 a), the kinetics of wear at 100°C is linear as predicted by Archard's law [1,21] showing a continuous abrasion of the surface. At 230°C, the wear kinetics displays a bilinear evolution. First, a fast increase with fretting cycles is observed until a critical number of cycles, $N_{crit,230°C}$ is achieved above which there is a plateau evolution. The fast increase at the beginning of the test may be related to the plastic deformation induced by a high hertzian pressure [1]. At 575°C, the transient stage is so short that only the plateau evolution is seen on the graph.

In Fig. 5 b), a strong effect of frequency is observed at 100°C: the higher the frequency, the lower the wear volume. This effect totally disappears at 230°C and 575°C. Moreover, wear volume at 1 Hz and 100°C (circled experimental point) is very low and does not follow the decreasing trend for higher frequencies. Optical image of this test reveals that the wear scar is covered by a bright layer as observed in domains II and III.

In Fig. 5 c), the evolution of wear volume with normal force displays a linear trend for the three studied temperatures. However, the slope of the linear trend is dependent on temperature.

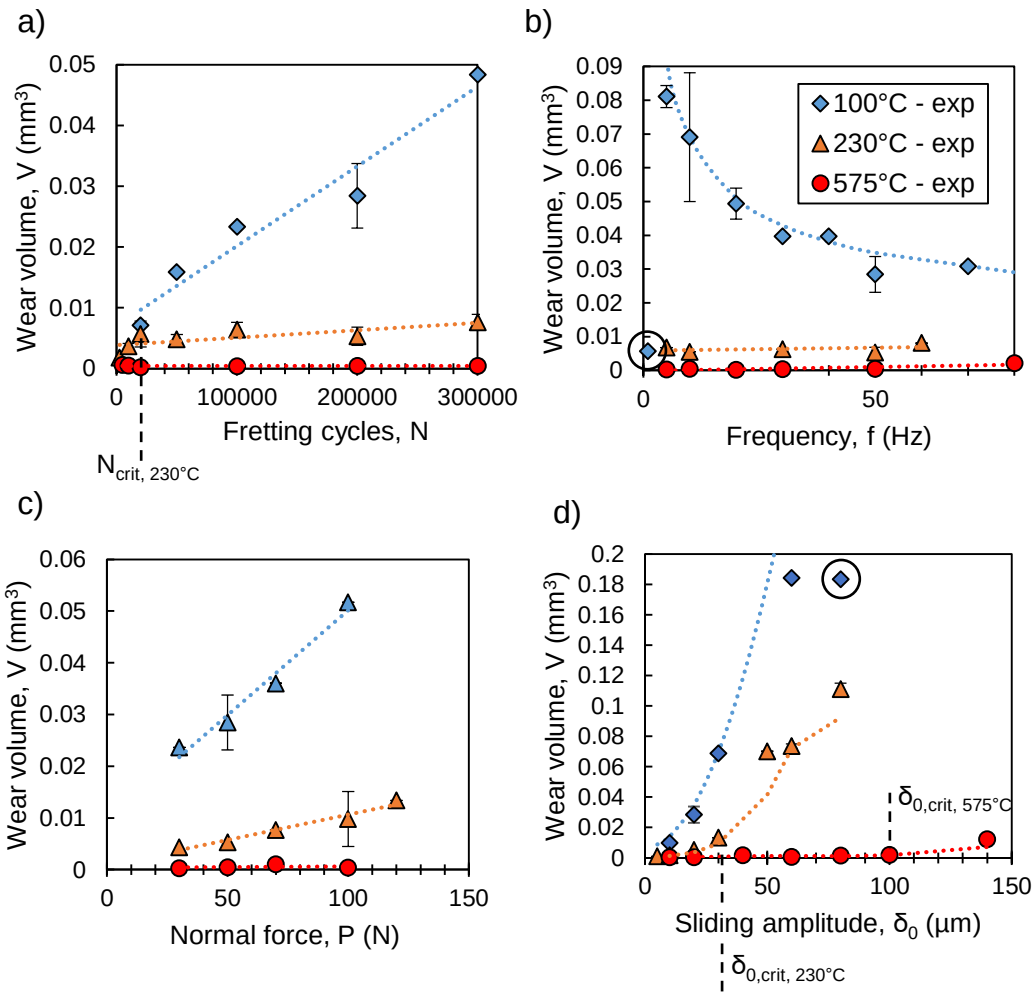

Fig. 5: Evolution of the wear volume with the variation of (a) fretting cycles, (b) frequency, (c) normal force and (d) sliding amplitude

Finally, in Fig. 5 d), the evolution of wear with sliding amplitude displays different trends at 100°C and 230°C - 575°C. At 100°C, the wear volume displays a sharp increase with the sliding amplitude. At 230°C and 575°C, the effect of the sliding amplitude is neglected until it reaches a critical amplitude $\delta_{0,crit}$ after which the wear increases. At 100°C, the circled point representative of $\delta_0 = \pm 80$ µm does not follow the increasing trend and it seems that a plateau evolution begins. This hypothetic evolution will be discussed in details later.

It is interesting to note that the major fluctuation appears between 100°C and 230°C, i.e. between domain I and II. Consequently, the T_1 transition may be considered as a key parameter for describing the HS25 fretting wear process.

3.3. Morphology and chemistry of fretting scars

Fig. 6 shows some cross-sections of wear scars after being fretted at a) 100°C, b) 230°C and c) 575°C. At 100°C, the third body layer is made of rather large agglomerated oxide debris with a mean size of 3 µm (see Fig. 6 a) and Table 2, spot A). In contrast, at 575°C, the third body layer is made of a very fine compacted oxide debris (Table 2, spot C). A sintered-like structure (glaze layer) is observed in Fig. 6 c) with no distinguishable particles, even using a high resolution SEM at high magnification. A

previous study showed, in TEM imaging, that the glaze layer created from HS25 debris is made of nanograins and some amorphous zones [15]. Finally, at 230°C, in Fig. 6 b), the interface displays a thin layer of oxide debris with distinguishable grains which seems to be a transitional form of compacted wear debris. It reveals that the interface and the associated tribolayer are very sensitive to the temperature even if both of these interfaces are oxidized, according to the EDX analysis presented in Table 2. Moreover, even if the third body layer displays some morphological differences between 230°C and 575°C, the wear kinetics plot on Fig. 5 a) shows that both of them are able to protect the contact from further wear.

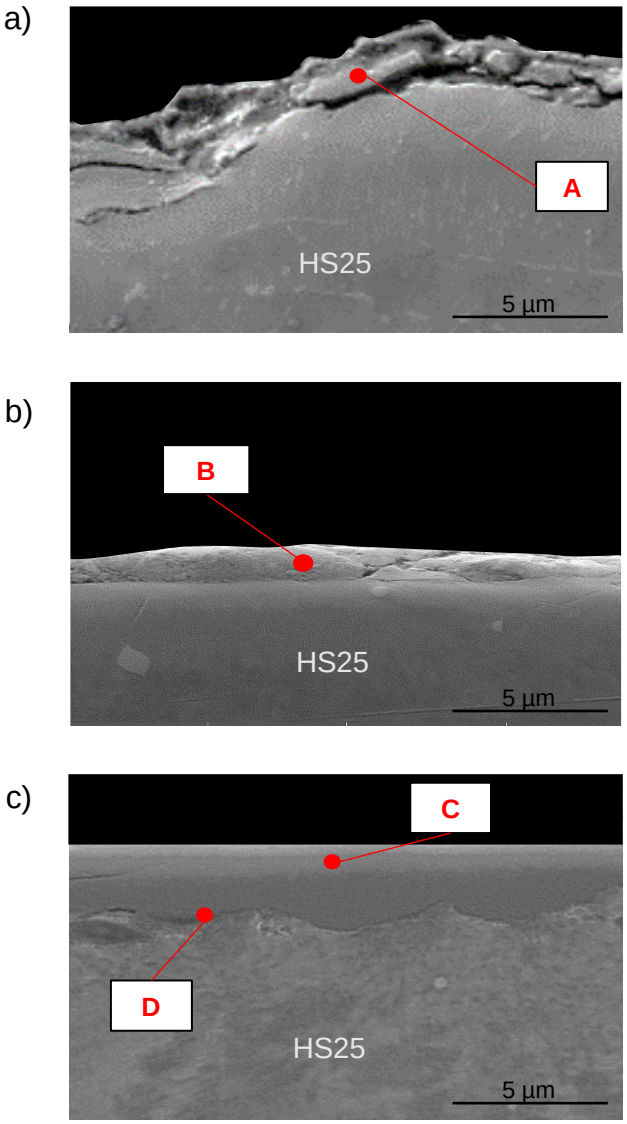

Fig. 6: SEM cross-section observations of wear scars at (a) 100°C – domain I, (b) 230°C - domain II and (c) 575°C - domain III.

Table 2: EDX analyses of the third bodies in cross-section (in wt. %)

Spot	Co	O	Ni	W	Cr
A (I : 100°C)	36.4 ± 6.82	29.4 ± 1.34	10.8 ± 0.99	9.35 ± 0.86	7.04 ± 4.39
B (II : 230°C)	31.2 ± 0.30	29.8 ± 0.31	6.18 ± 0.18	8.22 ± 0.41	12.5 ± 0.16
C (III : 575°C)	37.8 ± 1.03	33.3 ± 0.21	4.84 ± 0.09	6.76 ± 1.10	6.75 ± 0.36
D (III : 575°C)	26.1 ± 0.65	20.8 ± 0.77	7.36 ± 1.24	12.4 ± 0.04	25.9 ± 1.26

Fig. 7 presents Raman spectra acquired from different wear tracks fretted at 100°C, 230°C and 575°C. Spectra at 100°C and 575°C present the same signal envelop, with more pronounced peaks when temperature increases, which means that the oxides species may be the same irrespective of temperature. At 230°C, two peaks appear on the signal showing the presence of additional Cr_2O_3 oxides (around 283 and 330 cm^{-1} emphasized by *). EDX data presented in Table 2, spot B confirm an increase in the chromium content in the wear track at this temperature. However, all the spectra display a shape similar to that of the Co_3O_4 oxide, as reported by Viat & al [6]. The broader peaks can be explained by the presence of other structures like $CoCr_2O_4$, Cr_2O_3, $NiCr_2O_4$ or CoO oxides displaying Raman spectra similar to that of Co_3O_4. The small shift observed between the reference Co_3O_4 Raman peaks and the spectra measured in the fretting scar may also be explained by different aspects such as residual stress [22], size or quality of the crystalline system [23]. It may be easily assumed that the fretting loading induces defects in the crystals or reduces their size [14–16]. Therefore, we can conclude that the main oxides created during fretting may be Co_3O_4, with probably a mixture of other oxides or spinels with proportions depending on the operating temperature.

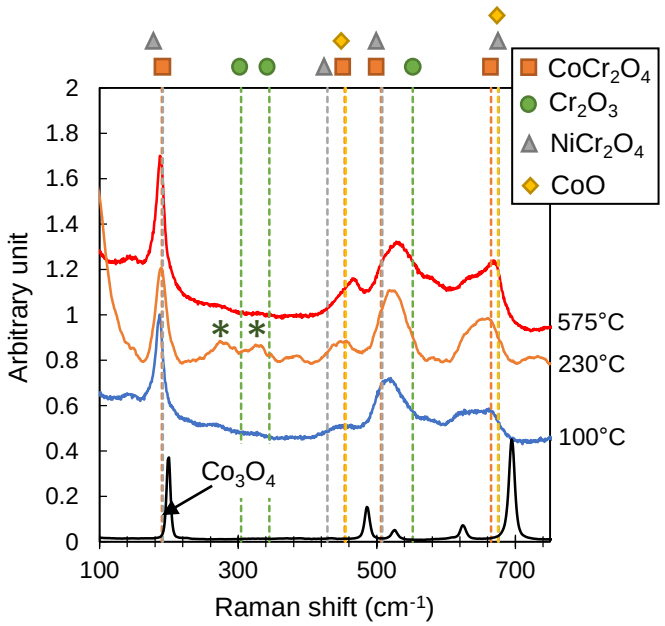

Fig. 7: Raman spectra of wear track at 100°C, 230°C and 575°C. Reference lines and the Co_3O_4 spectra are extracted from [6].

Some authors have shown the strong influence of oxide species on friction [4,24] and wear [12,25–27]. In the present work, the high friction coefficient at 230°C may be related to the presence of additional Cr_2O_3. This phenomenon has never been reported in the literature and some authors showed, on the contrary, the beneficial effect of Cr_2O_3 on both wear and friction [4]. The absence of

Cr_2O_3 at low temperature (100°C) is unexpected according to the thermodynamics principles since chromium is easily oxidized [28]. However, this may be explained by the diffusion of chromium at the surface to form Cr_2O_3 oxides which are then ejected by wear, and thus creating a vacancy of chromium (Table 2, spot A). At 575°C, the presence of a thin Cr-rich layer between the bulk metal and the glaze layer (Fig. 6 c) and Table 2, spot D) is commonly seen in static oxidation [29] as well as tribo-oxidation processes [9,30]. It can be explained by the diffusion of oxygen through the oxide scale (Co-rich, Table 2, spot C) which will easily reacts with the chromium at the oxide scale/bulk metal interface. The chemistry of the tribolayers need further investigation in future works.

However, it seems that the oxide species do not play a major role on the wear behavior since the Raman investigations showed rather similar spectra at 100°C and 575°C whereas wear volume was divided by 80. Then, the transition from severe-to-mild wear regime does not seem to be induced by a strong modification of the oxides structure but rather explained by a modification of the rheological properties of the debris layer as depicted in [6]. This rheological modification could be promoted by a sintering-like process between crystalline oxide particles as shown by the more pronounced Raman peaks at high temperature [23]. This phenomenon induces the formation and the consolidation of a compacted third body layer and leads to a full accommodation of the interfacial fretting strain by plastic flow [17] thus limiting further wear.

Temperature has a strong influence on wear and drastically changes the wear mechanism involved by altering the debris rheology. It is then important to be able to take into account the effect of the temperature to well formalize and understand the wear evolution of this tribosystem. In the following, an original and comprehensive energetic wear law is proposed in order to describe wear volume as a function of different tribological parameters, including temperature.

4. Wear energy description at low temperatures (T < 150°C)

4.1. Oxidative-abrasive wear

It has been previously found [1] that in domain I (T < 150°C), wear volume depends on both mechanical loadings and chemical reactions at the surface. As reported in tribocorrosion [31,32], the proposed scenario suggests that the wear process is controlled by a synergetic interaction between the oxidation of the metal and the abrasion of the latter by the sliding action of the hard alumina counterbody. This scenario explains the increase in wear with temperature in domain I by considering that temperature enhanced the growth of the oxide layer and therefore the amount of oxide wear debris. The scenario also proposed that the penetration of oxygen inside the contact is promoted by a reduction of frequency (inverse of the elapsed time between two fretting passes) and the increase in sliding amplitude. It has been concluded that the wear volume when the temperature is below T_1 may be expressed by Eq. 3 [1]:

$$V = V_\phi + K_{ox}\frac{1}{\sqrt{f}}\exp\left(\frac{-E_a}{2RT}\right)P\delta_0^2 N \quad (3)$$

Where V_ϕ is an offset of wear (mm^3) activated by the high plastic deformation at the beginning of the test, K_{ox} is a constant coefficient ($mm^2.s^{0.5}/J$), f is the frequency (Hz), E_a is the activation energy for the oxidation process (J/mol), R is the universal constant, T is the temperature (K), P is the normal

force applied on the tribosystem (N), δ_0 is the sliding amplitude (mm) and finally N is the number of fretting cycles. Eq. 3 was applied for a large number of fretting tests at low temperatures for various tribological parameters and it showed a very good prediction (the relative standard deviation was around 20%).

However, one limitation of the Archard's formulation as proposed in Eq. 3 is that the friction coefficient is not included in the wear rate description. Johnson [33] through the elastic-plastic shakedown chart clearly underlined the necessity to consider the friction coefficient when the friction coefficient is higher than 0.3 to formalize the surface damages and consequently the fretting wear rates. To better describe fretting wear, Mohrbacher [34] and Fouvry [35] proposed an energetic law where the interfacial shear work (equivalent to the friction energy) is the main driven factor of wear:

$$V = \alpha \sum E_d \tag{4}$$

Where α (mm^3/J) is the energetic wear coefficient. This law has been found to be performant for abrasive wear [5] as well as adhesive wear [19].

4.2. Introduction of a friction energy wear formulation

In this section, the oxidative-abrasive wear law (Eq. 3) is reformulated into a friction energy formalism. By combining Eq. 2 and Eq. 3 it leads to:

$$V = V_\phi + \frac{K_{ox}}{\sqrt{f}} exp\left(-\frac{E_a}{2RT}\right) \frac{\delta_0}{4\overline{\mu_e}} \sum E_d \tag{5}$$

Eq. 5 can be re written as:

$$V = V_\phi + \alpha_{ox} \Psi \sum E_d \tag{6}$$

Where:

$$\begin{cases} \alpha_{ox} = \frac{K_{ox}}{4\overline{\mu_e}} \\ \Psi = \frac{1}{\sqrt{f}} exp\left(-\frac{E_a}{2RT}\right) \delta_0 \end{cases} \tag{7}$$

An apparent energetic wear coefficient is then introduced:

$$\alpha^* = \alpha_{ox} \Psi \tag{8}$$

With α_{ox} ($mm^2.s^{0.5}/J$) an oxidational energetic wear coefficient, Ψ ($mm/s^{0.5}$) a tribo-oxidation parameter and α^* the apparent energetic wear coefficient in mm^3/J. Compared with the classical energetic wear formulation (Eq. 4), the presence of an additional term (Ψ) is related to the strong effect of the environment on the wear volume. Ψ represents both the chemical reactivity of the fretted surface with its environment and the enhanced environment reactivity influenced by the tribological parameters. Eq. 7 suggests the following conclusions:

- An increase in temperature enhances the oxidation process by allowing an enhanced diffusion of species through the oxide scale. Such an evolution is illustrated by an exponential rise of the Ψ parameter.

- An increase in frequency reduces the time allowed for the oxidation process to occur leading to an asymptotic reduction of Ψ.
- An increase in sliding amplitude induces a better contact oxygenation promoting a linear increase of Ψ.

4.3. Wear prediction in low temperature domain

The unknown parameters of Eq. 6 (V_ϕ, α_{ox} and E_a) need to be adjusted from experiments. Fig. 8 shows that the offset of wear V_ϕ can be found by a simple linear regression on the wear kinetics curve (Fig. 8 a)) and the activation energy for the oxidation process can be found by fitting an exponential equation to the wear volume – temperature curve (Fig. 8 b)). It is found that $V_{\phi,I}$ = 0.0071 mm^3 (R^2 = 0.95) and E_a = 36748 J/mol (R^2 = 0.97).

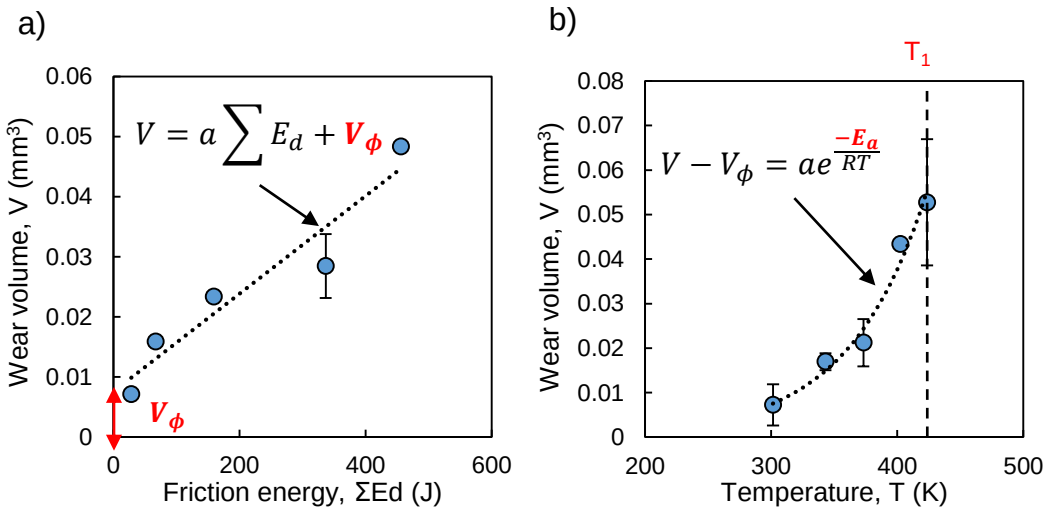

Fig. 8: Adjustment of the unknowns V_ϕ and E_a with (a) the wear volume versus fretting cycles curve (extracted from Fig. 5) at 100°C and (b) the wear volume versus temperature curve (extracted from Fig. 4).

Fig. 9 a) and b) show the experimental data collected in domain I. A rather large scattering is observed when the wear volume is plotted versus the cumulated dissipated energy (ie. V - ΣE_d system). It is clear that there is no linear trend, showing that the classical friction energy approach (Eq. 4) is not sufficient to describe the studied HS25/alumina fretting wear response in domain I. Fig. 9 b) plots the same experimental data versus the $\Sigma Ed \times \Psi$ parameter (related to Eq. 6). All the experimental points are now following a linear trend which can be approximated by:

$$V = V_{\phi,I} + \alpha_{ox,I}\Psi\sum E_d \quad (9)$$

With $\alpha_{ox,I}$ = 10.7 mm².s$^{0.5}$/J (R^2 = 0.97). The two circled points are those from Fig. 5 and were not taken into consideration for the calculations.

Fig. 9 c) presents data from domain II (triangles) and III (circles) plotted versus the cumulated dissipated energy and Fig. 9 d) versus the $\Sigma Ed \times \Psi$ formulation. In contrast, the wear volume extension for domains II and III displays a larger discrepancy even using the $\Sigma Ed \times \Psi$ formulation. This suggests that, similarly to a lubricated interface [36,37], an alternative effective friction energy must be considered when an accommodating tribolayer is formed.

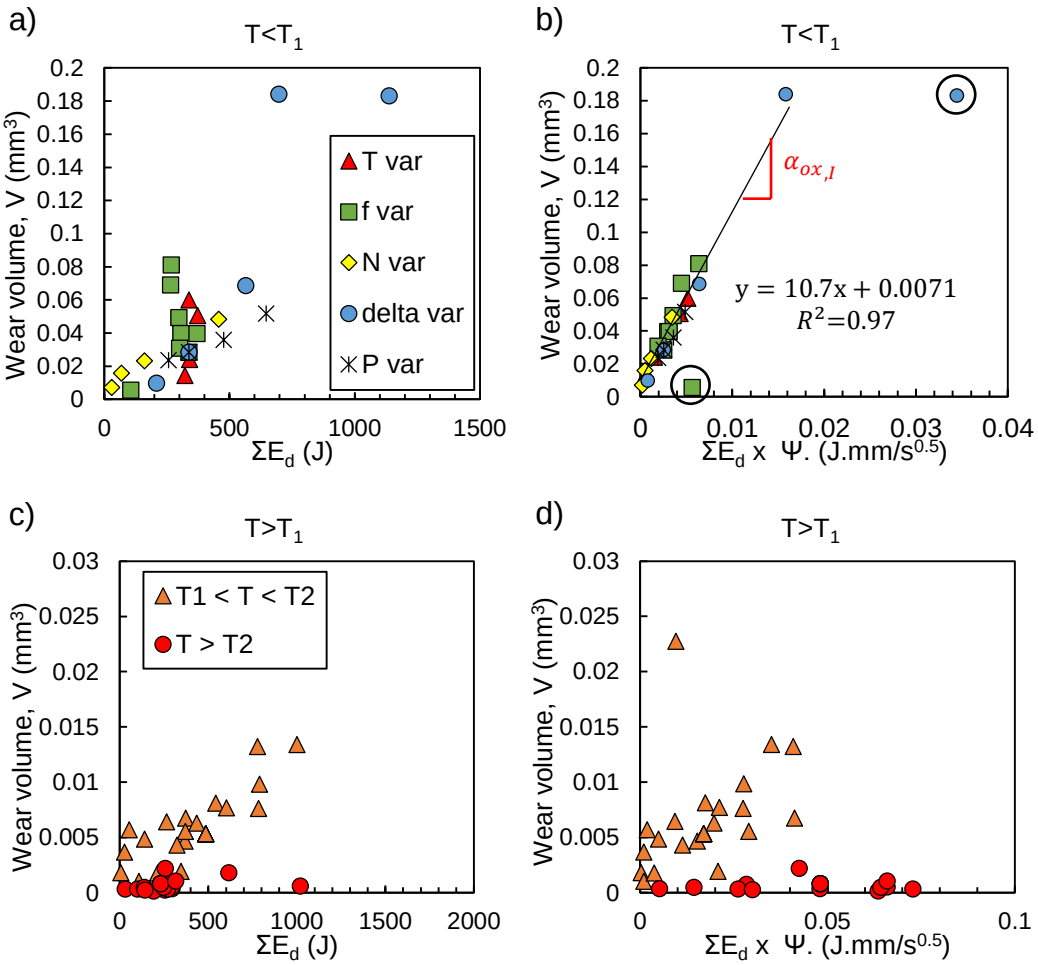

Fig. 9: Evolution of wear volume as a function of the cumulated dissipated energy in (a) domain I ($T<T_1$) and (c) domains II & III ($T>T_1$) and with respect to the tribochemical weighted cumulated dissipated energy in (b) domain I and in (d) domains II & III, with T_1 = 150°C and T_2 = 400°C.

5. Introduction of an effective friction energy for wear prediction at high temperature

5.1. Wear transition from low to high temperatures

Fig. 10 shows the evolution of wear scars with fretting cycles at 100°C (Fig. 10 a)) and at 230°C (Fig. 10 b)). At 100°C, the wear scar morphology remains the same over the cycles meaning that the abrasive-oxidative process takes place irrespective of the wear track extension. At 230°C, a rather performant compliant and bright third body is formed and covers the interface. Fig. 10 b) shows that this glaze layer is extended over fretting cycles: 29% of the total fretted area is covered at N = 10 000 whereas more than 80% of the surface is covered for N > 100 000. To quantify such a transition, the critical number of fretting cycle N_{crit} introduced in Fig. 5 a) is reported on Fig. 10 b). It shows that the plateau evolution on Fig. 5 a) is directly related to a large enough area of glaze layer which is able to consume a major part of the friction energy by plastic deformation instead of wear. In the following,

N_{crit} is assumed to be equal to N_{GL} which is the number of cycles necessary to form a protective glaze layer. It has been demonstrated that N_{GL} is dependent on temperature and that the more the temperature increases, the more N_{GL} decreases [38].

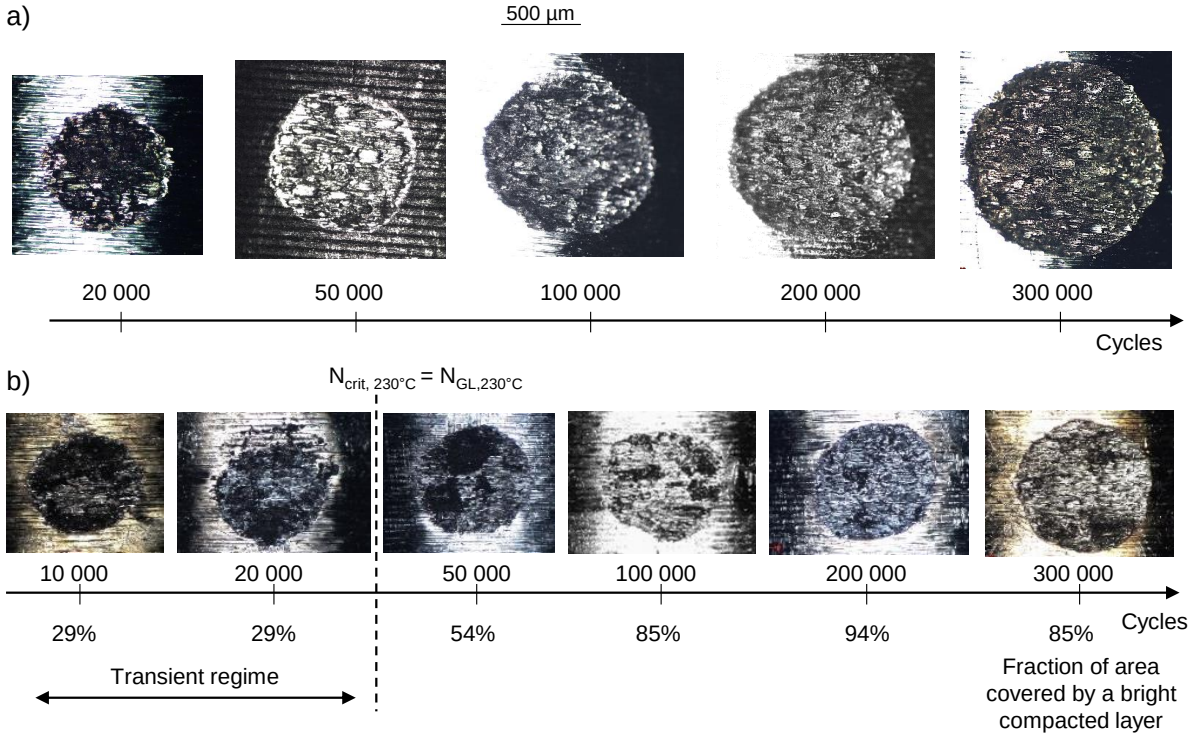

Fig. 10: Evolution of wear scars during fretting wear at (a) 100°C and (b) 230°C

It is also interesting to note on Fig. 10 that at the beginning of the tests (N < 20 000), for both temperatures, the morphology of the wear tracks are very similar, with the presence of some black oxides. Then, a similar wear process may be assumed between domain I (100°C) and the transient regime of domain II (230°C).

Fig. 11 presents the wear kinetics for the three reference temperatures in the V - $\Sigma Ed \times \Psi$ system. At 230°C, before the plateau evolution, wear displays a linear trend which can be related to an abrasive process. When the critical number of cycle is reached, the plateau evolution begins and the wear evolution is negligible. Then, an effective friction energy $\Sigma E_{d,eff}$ can be related to the N_{GL} cycle, after which the friction energy is no more consumed by wear but rather by plastic accommodation of the tribolayer. This analysis is extended to the high temperatures. Fig. 11 also demonstrates that the energetic wear coefficient is different between domain I (100°C), domain II (230°C) and domain III (575°C) which can be explained by a limited wear due to the presence of some protective third body islets even before the N_{GL} transition. In the following, three energetic wear coefficients will be considered: $\alpha_{ox,I}$ for domain I : $T < T_1 = 150°C$, $\alpha_{ox,II}$ for domain II : $T_1 < T < T_2 = 400°C$ and $\alpha_{ox,III}$ for domain III : $T > T_2$.

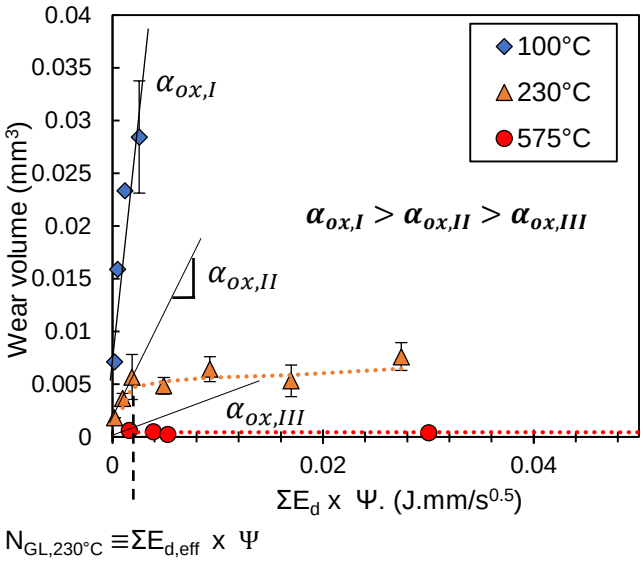

Fig. 11: Comparison of the wear kinetics of the three domains with the $\Sigma E_d \times \Psi$ parameter

Wear rates in domain II and III are controlled by the glaze layer formation. When the glaze layer is formed, all the friction energy is consumed by the latter and there is no additional wear. This is observed in Fig. 5 a) and Fig. 11 where, instead of a linear wear extension as seen in domain I (100°C), domain II and III are characterized by a plateau evolution as soon as the glaze layer is formed. From this analysis we can conclude that wear in domain II and III is generated during the transient period before the effective glaze layer protection (N_{GL}) and may be predicted using the oxido-abrasive wear law (Eq. 6). Hence, to predict the wear volume extension in domains II and III, we need to identify N_{GL} and its related dissipated friction energy $\Sigma E_{d,eff}$.

5.2. Introduction of a threshold fretting cycle N_{GL}

One strategy to identify N_{GL} is to consider a "sintering-like" approach. Many authors considered that the main driving factor of the glaze layer formation is a tribo-sintering process of the oxide debris [11,12]. Different studies on the glaze layer formation showed that the partial oxygen pressure [39], the temperature or the frequency [38] have a strong effect on its formation. This results are very similar to the sintering process of powder where, at iso-pressure, the shrinkage rate depends on the atmosphere, the heating temperature and the process time [40,41].

Moreover, some previous investigations [6,12,42] showed that the capacity of the HS25 to create a glaze layer is principally due to the capacity of cobalt to diffuse easily through the oxide scale, thickening the oxide layer and so as welding the grains together and starting the sintering process. It was emphasized that the glaze layer formation is driven by kinetics more than thermodynamics considerations [6]. Then, we consider that the formation of the glaze layer is directly related to the oxidation rate of the alloy through an Arrhenius law:

$$k_p = k_{p0} exp\left(-\frac{E_a}{RT}\right) \quad (10)$$

Where k_p (mm²/s) is the oxidation rate and k_{p0} (mm²/s) is a pre-exponential constant. It was shown that for a contact subjected to fretting solicitation, the amount of oxygen available at the interface is

function of the sliding amplitude which control the ambient air exposure of the interface [1]. A relation is then assumed in Eq. 11:

$$k_{p0} \propto \delta_0^n \tag{11}$$

A very good correlation has been found when n=2 for a cross-cylinders contact [1].

Then,

$$k_p \propto \delta_0^2 exp\left(-\frac{E_a}{RT}\right) \tag{12}$$

Another parameter controlling the oxidation and the sintering processes is the amount of time during which the particles are held against each other ($t_{holding}$). Then, the glaze layer formation is assumed to be controlled by a tribo-sintering process and is efficient only when a sintering rate threshold is achieved. Hence, a sintering parameter S is introduced so that the debris sintering process is activated if $S \geq S_{GL}$. We define S as follows:

$$S = t_{holding} \times k_p \tag{13}$$

Which implies

$$S = \frac{N}{f}\delta_0^2 \, exp\left(\frac{-E_a}{RT}\right) \tag{14}$$

With $t_{holding} = N/f$ and $E_a = 36748$ J/mol. Fig. 12 plots the evolution of S (Eq. 13) as a function of $V/\Sigma E_d$ using the same data set as that of Fig. 4 and Fig. 5. Fig. 12 shows the presence of a threshold value S_{GL} leading to a differentiation of domain I from domains II and III ($S_{GL} = 9.5 \times 10^{-5}$ mm^2/s). The two circled points are those defined in section 3.2 and their sintering parameters S are higher than S_{GL} which confirms that they do not follow an abrasive-oxidative wear process even at low temperature. On the other hand, the transient regime at 230°C is clearly illustrated on Fig. 12 and it shows that $S < S_{GL}$. The mild wear regime is activated when $S \geq S_{GL}$.

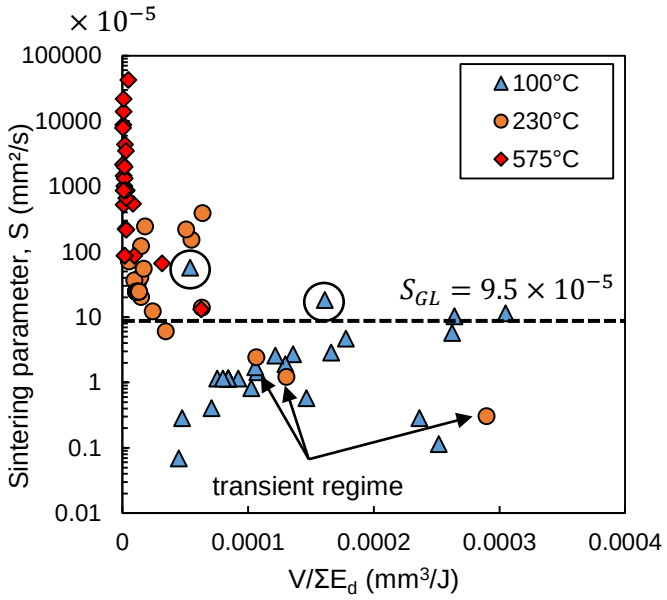

Fig. 12: Classification of experimental data from Fig. 4 and Fig. 5 according to their sintering parameter S

With Eq. 14, the number of cycle N_{GL} related to the formation of the glaze layer can be extrapolated and expressed from the other tribological conditions (T, f, δ_0):

$$N_{GL} = \frac{S_{GL}}{\delta_0^2 \exp(-\frac{E_a}{RT})} f \quad (15)$$

According to Eq. 15, it is possible to map the glaze layer formation thanks to the $N \geq N_{GL}$ condition for several parameters (δ_0, f, T) in the form of maps. An example of glaze layer formation map is plotted on Fig. 13. Fig. 13 shows that the glaze layer formation (when $N \geq N_{GL}$) is strongly dependent on temperature: when the temperature decreases, N_{GL} increases drastically. This confirms the strong relation between the glaze layer formation and temperature as experimentally demonstrated by some authors [38].

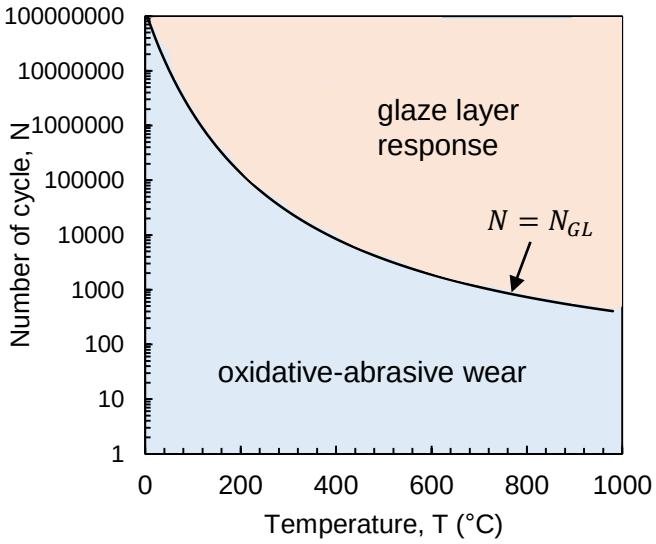

Fig. 13: Map of the glaze layer formation when the temperature varies (P = 50 N; f = 50 Hz; δ_0 = ± 20 µm)

5.3. Introduction of an effective friction energy concept

In this section, an effective friction energy is introduced in order to calculate the wear volume in domains II and III when a glaze layer is created over the fretting cycles. An energetic wear formulation is considered before the glaze layer protective effect is activated, that is to say before N_{GL} is reached. The friction energy is then the sum of the dissipated energy until N_{GL} instead of the total number of fretting cycles N (effective cumulated friction energy).

Moreover, this formulation needs to take into account the different kinetics of wear depending on temperature (Fig. 11):

$$\alpha_{ox,I} > \alpha_{ox,II} > \alpha_{ox,III} \quad (16)$$

The decrease in energetic wear coefficient with temperature may be explained by several hypotheses. First, during the transient phase in domains II and by extension III, the debris are not fully ejected from the interface due to the adhesion of particles increasing with temperature [10] and locally, some glaze layer islets can protect the interface. Then, the global energetic wear coefficient is lower when some lubricant islets are present. Second, an increased temperature may promote

plastic deformation of the bulk allowing a better entrapment of wear debris inside the wear track [43] and thus decreasing the wear rate and the energetic wear coefficient.

A global energetic wear law is then proposed:

$$V = V_{\phi}(T) + \alpha_{ox}(T)\Psi\sum_{i=1}^{N_{eff}} E_{d,i} = V_{\phi}(T) + \alpha^{*}\sum E_{d,eff} \quad (17)$$

With

$$N_{eff} = \begin{cases} N \; if \; N < N_{GL} \\ N_{GL} \; if \; N > N_{GL} \end{cases} \quad (18)$$

$$\alpha_{ox}(T) = \begin{cases} \alpha_{ox,I} \; if \; T<T_1 \\ \alpha_{ox,II} \; if \; T_1<T<T_2 \\ \alpha_{ox,III} \; if \; T>T_2 \end{cases}$$

5.4. Validation of the friction energy model and discussion

Table 3 recapitulates the parameters used in Eq. 17 for the validation of the model. Fig. 14 displays a comparison between analytical results from Eq. 17 and the experiments from Fig. 4 b). It shows a very good correlation. This model allows to conservatively estimate the wear volume for temperatures ranging from ambient to 600°C.

Table 3: Calculation of various parameters for Eq. 21

Domain	Wear offset V_{ϕ} (mm^3)	Energetic wear coefficient α_{ox} ($mm^2.s^{0.5}/J$)	Activation energy for oxidation process E_a (J/mol)
I ($T < T_1$)	0.0071	10.7	36748
II ($T_1 < T < T_2$)	0.0013	1.4	36748
III ($T > T_2$)	0	0.065	36748

The model presented in Eq. 17 well captures the two following effects:

- The increase in apparent energetic coefficient of wear α^{*} with temperature due to the elevation of the tribo-oxidation parameter Ψ (Eq. 7)
- The decrease in effective friction energy $\Sigma E_{d,eff}$ due to the formation of a compliant third body when the embedded debris starts to sinter together lowering the effective number of cycles of the wear process (Eq. 15).

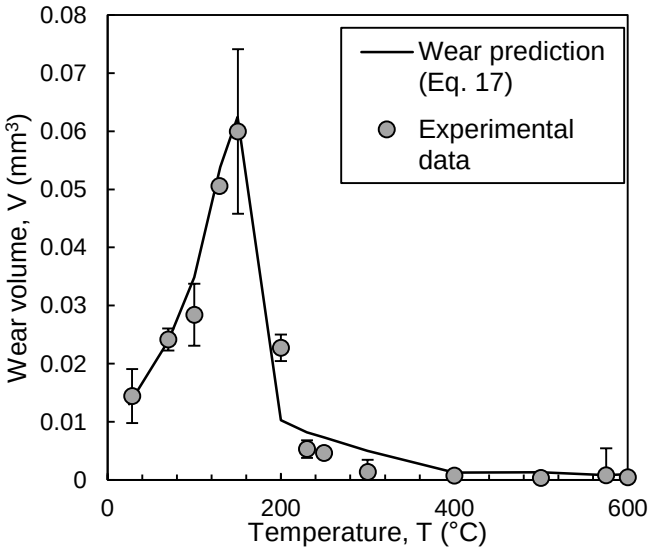

Fig. 14: Comparison between experiments and theoretical calculation for various temperatures (the other parameters are fixed to their reference)

Moreover, this formulation is able to estimate wear volume as a function of sliding amplitude, frequency, normal force and number of fretting cycle as showed in Fig. 15.

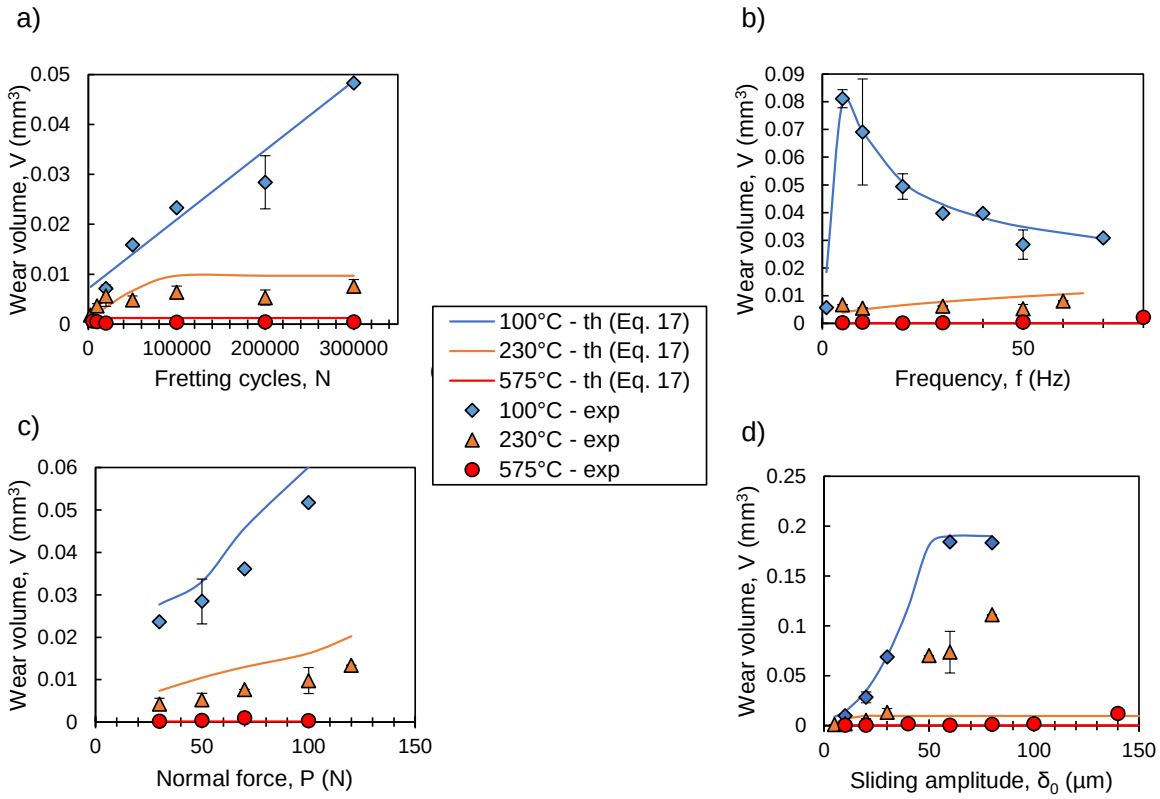

Fig. 15 : Theoretical parametric study for three temperatures : 100°C, 230°C and 575°C when (a) the number of cycle, (b) the frequency, (c) the normal force and (d) the sliding amplitude vary

On Fig. 15 a), the linearity of the wear kinetics is respected at 100°C as well as the bi-linearity at 230°C and 575°C. At 100°C, the N_{GL} value is never achieved (at least for N = 300 000) showing that the

protective third body cannot be formed. Then, the friction energy is fully consumed by wear leading to the linear evolution of the wear volume. On the contrary, at 230°C and 575°C, N_{GL} is reached meaning that at this point, a protective third body is formed.

On Fig. 15 b), the formulation well describes at 100°C the reduction of wear with frequency due to a diminution of the oxide debris production. Moreover, the lower point at 1 Hz is now captured and wear volume is well estimated. For higher temperatures, the sintering process takes place irrespective of frequency leading to a very smooth increase in wear with frequency.

It is interesting to notice for the normal force variation, on Fig. 15 c), that the law well captures the evolution of wear as a function of normal force at different temperatures. This sensitivity to normal force variations is directly due to the change of the apparent energetic wear coefficient α^* as well as the experimental value of $\overline{\mu_e}$.

Finally, on Fig. 15 d), at 100°C, the power dependence of wear volume with the sliding amplitude is respected. Moreover, the plateau evolution starting for a sliding amplitude equal to 60 µm is now integrated in the formulation. This constant wear volume is based on a competition between an increased debris production and an enhanced sintering rate. At 230°C and 575°C, there is a pretty good correlation but $\delta_{0,crit}$ as defined on Fig. 5 is not taken into consideration in the formulation and needs further investigations.

This complex energetic wear law displays good results compared with experiments and tends to confirm the hypothesis made in this research work. However, the model has its own limits:

- The S_{GL} value is found experimentally but its physical dependences are not yet highlighted. This value is likely dependent on the material considered (oxidation rate, diffusion property) but also on the size of the wear debris particles. Moreover, the normal force is not included in the formulation of S_{GL}.
- The energetic wear coefficient α_{ox} is a discrete function of the temperature but should be a continuous function since the presence of some early glaze layer islets increases with temperature. It is also assumed to be dependent only on the temperature but the other tribological parameters may have an effect on it.
- It is also quite difficult to estimate the wear offset V_ϕ due to the severe plastic deformation at the beginning of the test. Here, it is proposed that this offset is only due to the temperature variation which is not totally true and may also be dependent on the sliding distance [1]. This kind of “run-in” wear volume is difficult to capture and predict.
- The effect of contact size is not taken into consideration. Some studies showed the role of the contact size in the debris ejection flow and the oxygen accessibility [19,44].

6. Conclusion

This research work demonstrates that the wear volume evolution of a cobalt-based alloy (HS25) is monitored by a synergetic interaction between the friction energy concept, a tribo-oxidation process and the activation of a so-called glaze layer. Fig. 16 illustrates the principle of the wear model developed in this research work.

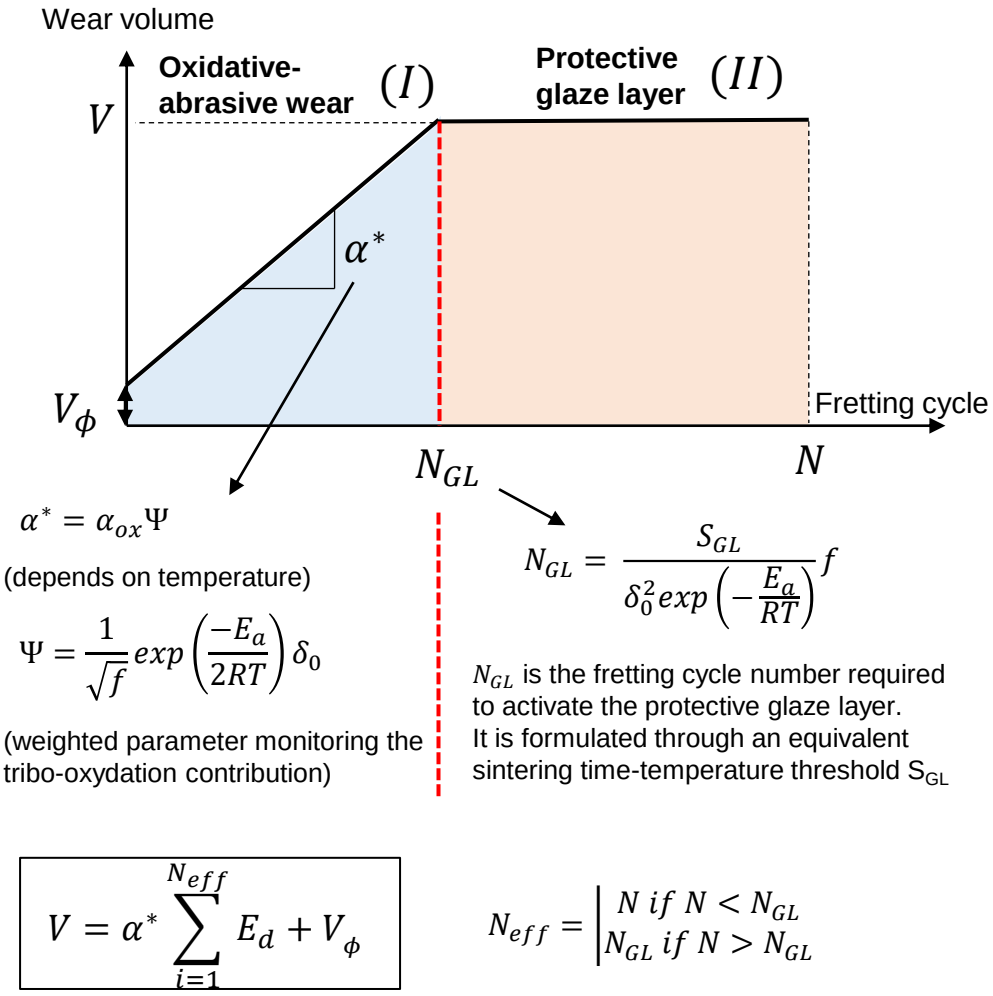

Fig. 16 : Schematic illustration of the proposed wear model

The wear volume is described through a bilinear evolution. Before the glaze layer activation ($N < N_{GL}$), the wear volume is proportional to the friction energy dissipated at the interface weighted by the effect of the corrosive environment (linear phase I). When the glaze layer is formed ($N>N_{GL}$), no additional wear is generated (linear phase II) and the friction energy is dissipated in the accommodating third body. Hence, in order to estimate the total wear volume, it is necessary to extrapolate the N_{GL} fretting cycle threshold. This investigation shows that, similarly to powder sintering processes, the glaze layer formation can be estimated by a so called time-temperature dependency. A glaze layer sintering parameter is then introduced so that when $S = S_{GL}$ ($N=N_{GL}$), the glaze layer is formed.

Moreover, even during the linear phase I, the wear rate was shown to be a combined function of the mechanical loading and the corrosive environment (modelled by the tribo-oxidation parameter Ψ). The Ψ parameter was derived from a time (i.e. frequency)-temperature dependence combined with the effect of the sliding amplitude and influence the surface oxidation during the wear process.

Despite the relative simplicity of the model and the limited number of unknowns (α_{ox}, E_a, S_{GL}), a very good correlation was observed with the experiments. Many other aspects need to be considered to confirm this glaze layer wear model. For instance, the nature of the alloy and its composition may influence the three unknown variables. Besides, the model considers that when the glaze layer is

formed, there is no additional wear. Future works need to focus on this aspect and consider for example the fatigue cracking process of the glaze layer during fretting loads.

References

[1] A. Dreano, S. Fouvry, G. Guillonneau, A tribo-oxidation abrasive wear model to quantify the wear rate of a cobalt-based alloy subjecting to fretting in low to medium temperature conditions, Tribol. Int. 125 (2018) 128–140. doi:https://doi.org/10.1016/j.triboint.2018.04.032.

[2] B. Van Peteghem, S. Fouvry, J. Petit, Effect of variable normal force and frequency on fretting wear response of Ti-6Al-4V contact, Wear. 271 (2011) 1535–1542. doi:10.1016/j.wear.2011.01.060.

[3] A. Viat, S. Fouvry, M.I. De Barros Bouchet, L. Pin, Influence of carbon-based solid lubricant on fretting wear response for alumina-based ceramics versus cobalt superalloy contact, Surf. Coatings Technol. 284 (2015) 327–333. doi:10.1016/j.surfcoat.2015.07.043.

[4] A. Korashy, H. Attia, V. Thomson, S. Oskooei, Characterization of fretting wear of cobalt-based superalloys at high temperature for aero-engine combustor components, Wear. 330 (2015) 327–337. doi:10.1016/j.wear.2014.11.027.

[5] R. Rybiak, S. Fouvry, B. Bonnet, Fretting wear of stainless steels under variable temperature conditions: Introduction of a “composite” wear law, Wear. 268 (2010) 413–423. doi:10.1016/j.wear.2009.08.029.

[6] A. Viat, A. Dreano, S. Fouvry, M.-I. De Barros Bouchet, J.-F. Henne, Fretting wear of pure cobalt chromium and nickel to identify the distinct roles of HS25 alloying elements in high temperature glaze layer formation, Wear. 376–377 (2017) 1043–1054. doi:10.1016/j.wear.2017.01.049.

[7] J. Jiang, F.H. Stott, M.M. Stack, A generic model for dry sliding wear of metals at elevated temperatures, Wear. 256 (2004) 973–985. doi:10.1016/j.wear.2003.09.005.

[8] F.H. Stott, J. Glascott, G.C. Wood, The sliding wear of commercial Fe-12%Cr alloys at high temperature, Wear. 101 (1985) 311–324.

[9] F.H. Stott, D.S. Lin, The structure and mechanism of formation of the “glaze oxide layers” produced on nickel-based alloy during wear at high temperatures, Corros. Sci. 13 (1973) 449–469.

[10] J. Jiang, F.H. Stott, M.M. Stack, The role of triboparticulates in dry sliding wear, Tribol. Int. 31 (1998) 245–256. doi:10.1016/S0301-679X(98)00027-9.

[11] K. Adachi, K. Kato, Formation of smooth wear surfaces on alumina ceramics by embedding and tribo-sintering of fine wear particles, Wear. 245 (2000) 84–91. doi:10.1016/S0043-1648(00)00468-3.

[12] H. Kato, K. Komai, Tribofilm formation and mild wear by tribo-sintering of nanometer-sized oxide particles on rubbing steel surfaces, Wear. 262 (2007) 36–41. doi:10.1016/j.wear.2006.03.046.

[13] W.M. Rainforth, A.J. Leonard, C. Perrin, A. Bedolla-Jacuinde, Y. Wang, H. Jones, Q. Luo, High resolution observations of friction-induced oxide and its interaction with the worn surface, Tribol. Int. 35 (2002) 731–748. doi:10.1016/S0301-679X(02)00040-3.

[14] C. Rynio, H. Hattendorf, J. Klöwer, G. Eggeler, On the physical nature of tribolayers and wear debris after sliding wear in a superalloy/steel tribosystem at 25 and 300°C, Wear. 317 (2014) 26–38. doi:10.1016/j.wear.2014.04.022.

[15] A. Viat, M.-I. De Barros Bouchet, B. Vacher, T. Le Mogne, S. Fouvry, J.-F. Henne, Nanocrystalline glaze layer in ceramic-metallic interface under fretting wear, Surf. Coatings Technol. 308 (2016) 307–315. doi:10.1016/j.surfcoat.2016.07.100.

[16] T.W. Scharf, S. V. Prasad, P.G. Kotula, J.R. Michael, C. V. Robino, Elevated temperature tribology of cobalt and tantalum-based alloys, Wear. 330–331 (2015) 199–208. doi:10.1016/j.wear.2014.12.051.

[17] A. Viat, G. Guillonneau, S. Fouvry, G. Kermouche, S. Sao, J. Wehrs, J. Michler, J. Henne, Brittle to ductile transition of tribomaterial in relation to wear response at high temperatures, Wear. 392–393 (2017) 60–68. doi:10.1016/j.wear.2017.09.015.

[18] S. Fouvry, P. Kapsa, An energy description of hard coating wear mechanisms, Surf. Coatings Technol. 138 (2001) 141–148. doi:10.1016/S0257-8972(00)01161-0.

[19] S. Fouvry, P. Arnaud, A. Mignot, P. Neubauer, Contact size, frequency and cyclic normal force effects on Ti-6Al-4V fretting wear processes : An approach combining power and contact oxygenation, Tri. (2017).

[20] Haynes International, HAYNES 25 alloy, 2004.

[21] J.F. Archard, Contact and rubbing of flat surfaces, J. Appl. Phys. 24 (1953) 981–988. doi:10.1063/1.1721448.

[22] C.A. Taylor, M.F. Wayne, W.K.S. Chiu, Residual stress measurement in thin carbon films by Raman spectroscopy and nanoindentation, Thin Solid Films. 429 (2003) 190–200. doi:10.1016/S0040-6090(03)00276-1.

[23] F. Adar, Raman Spectra of Metal Oxides, Spectroscopy. 29 (2014) 14–22.

[24] R.T. Foley, M.B. Peterson, C. Zapf, Frictional Characteristics of Cobalt, Nickel, and Iron as Influenced by Their Surface Oxide Films, A S L E Trans. 6 (1963) 29–39. doi:10.1080/05698196308971996.

[25] H. Kato, Severe-mild wear transition by supply of oxide particles on sliding surface, Wear. 255 (2003) 426–429. doi:10.1016/S0043-1648(03)00077-2.

[26] A. Iwabuchi, The role of oxide particles in the fretting wear of mild steel, Wear. 151 (1991) 301–311. doi:10.1016/0043-1648(91)90257-U.

[27] P.L. Hurricks, The fretting wear of mild steel from 200°C to 500°C, Wear. 30 (1974) 189–212. doi:10.1016/0043-1648(74)90175-6.

[28] T. Richardson, B. Cottis, D. Scantlebury, R. Lindsay, S.B. Lyon, M. Graham, Shreir's Corrosion - Volume I, 2010. doi:10.1016/C2009-1-28357-2.

[29] P.K. Kofstad, A.Z. Hed, High-Temperature Oxidation of Co-10 w / o Cr Alloys, J. Electrochem. Soc. 116 (1969) 224–229.

[30] C. Rynio, H. Hattendorf, J. Klöwer, G. Eggeler, The evolution of tribolayers during high temperature sliding wear, Wear. 315 (2014) 1–10. doi:10.1016/j.wear.2014.03.007.

[31] M. Keddam, F. Liao, P. Ponthiaux, V. Vivier, New advances in triboelectrochemistry: from steady state to impedance of abraded stainless steel in acidic medium, J. Solid State Electrochem. 19 (2015) 2591–2599. doi:10.1007/s10008-015-2914-8.

[32] S. Cao, S. Mischler, Modeling tribocorrosion of passive metals – A review, Curr. Opin. Solid State Mater. Sci. 22 (2018) 127–141. doi:10.1016/j.cossms.2018.06.001.

[33] K.L. Johnson, Contact mechanics and the wear of metals, Wear. 190 (1995) 162–170. doi:10.1016/0043-1648(95)06665-9.

[34] H. Mohrbacher, B. Blanpain, J.P. Celis, J.R. Roos, L. Stals, M. Van Stappen, Oxidational wear of TiN coatings on tool steel and nitrided tool steel in unlubricated fretting, Wear. 188 (1995) 130–137. doi:10.1016/0043-1648(95)06637-3.

[35] S. Fouvry, P. Kapsa, L. Vincent, Elastic-plastic shakedown analysis of fretting wear, Wear. 247 (2001) 41–54. doi:10.1016/S0043-1648(00)00508-1.

[36] S. Fouvry, C. Paulin, S. Deyber, Impact of contact size and complex gross-partial slip conditions on Ti-6Al-4V/Ti-6Al-4V fretting wear, Tribol. Int. 42 (2009) 461–474. doi:10.1016/j.triboint.2008.08.005.

[37] S. Fouvry, C. Paulin, T. Liskiewicz, Application of an energy wear approach to quantify fretting contact durability: Introduction of a wear energy capacity concept, Tribol. Int. 40 (2007) 1428–1440. doi:10.1016/j.triboint.2007.02.011.

[38] J. Glascott, G.C. Wood, F.H. Stott, The Influence of Experimental Variables on the Development and Maintenance of Wear-Protective Oxides during Sliding of High-Temperature Iron-Base Alloys, Proc. Inst. Mech. Eng. Part C J. Mech. Eng. Sci. 199 (1985) 35–41. doi:10.1243/PIME_PROC_1985_199_088_02.

[39] F.H. Stott, G.C. Wood, The influence of oxides on the friction and wear of alloys, Tribol. Int. 11 (1978) 211–218. doi:10.1016/0301-679X(78)90178-0.

[40] B. Paul, D. Jain, S.P. Chakraborty, I.G. Sharma, C.G.S. Pillai, A.K. Suri, Sintering kinetics study of mechanically alloyed nanocrystalline Mo-30 wt.% W, Thermochim. Acta. 512 (2011) 134–141. doi:10.1016/j.tca.2010.09.015.

[41] B. Paul, D. Jain, A.C. Bidaye, I.G. Sharma, C.G.S. Pillai, Sintering kinetics of submicron sized cobalt powder, Thermochim. Acta. 488 (2009) 54–59. doi:10.1016/j.tca.2009.01.017.

[42] F.H. Stott, Role of oxidation in the wear of alloys, Tribol. Int. 31 (1998) 61–71. doi:10.1016/S0301-679X(98)00008-5.

[43] J.D. Lemm, A.R. Warmuth, S.R. Pearson, P.H. Shipway, The influence of surface hardness on the fretting wear of steel pairs-Its role in debris retention in the contact, Tribol. Int. 81 (2014) 258–266. doi:10.1016/j.triboint.2014.09.003.

[44] S. Fouvry, R. Merhej, Introduction of a power law formulation to quantify the contact size effects on friction and wear responses of dry oscillating sliding contacts: Application to a chromium steel interface, Wear. 301 (2013) 34–46. doi:10.1016/j.wear.2013.01.072.

Acknowledgements

The authors would like to thank Damien Augarde (Ecole Centrale de Lyon) for performing the medium temperature tests used in this study. This research did not receive any specific grant from funding agencies in the public, commercial, or not-for-profit sectors.